AFRL-RH-FS-TR-2024-0001

Non-Fourier Laser-Tissue Heating Analysis: A Bio-heat Transfer Equation Comparison

Sara Botelho-Andrade
Elharith M. Ahmed
Matthew G. Seman
SAIC, Inc.

Andrew W. Wharmby
Raniero A. Lara-Garduno
711th Human Performance Wing
Human Effectiveness Directorate
Bioeffects Division
Optical Radiation Bioeffects Branch

18 November 2023

Interim / Final Report - June 2023 - September 2023

Air Force Research Laboratory
711th Human Performance Wing
Human Effectiveness Directorate
Bioeffects Division
Optical Radiation Bioeffects Branch
JBSA Fort Sam Houston, Texas 78234

NOTICE AND SIGNATURE PAGE

Using Government drawings, specifications, or other data included in this document for any purpose other than Government procurement does not in any way obligate the U.S. Government. The fact that the Government formulated or supplied the drawings, specifications, or other data does not license the holder or any other person or corporations; or convey any rights or permission to manufacture, use, or sell any patented invention that may relate to them.

This report was cleared for public release by the AFRL Public Affairs Office and is available to the general public, including foreign nationals. Copies may be obtained from the Defense Technical Information Center (DTIC) (http://www.dtic.mil).

"Non-Fourier Laser-Tissue Heating Analysis: A Bio-heat Transfer Equation Comparison "

(AFRL-RH-FS-TR- 2024- 0001) has been reviewed and is approved for publication in accordance with assigned distribution statement.

FERRIS.LYNDSEY.MARIE.1381070391 Digitally signed by FERRIS.LYNDSEY.MARIE.1381070391 Date: 2024.02.01 08:53:54 -06'00'

LYNDSEY M. FERRIS, LtCol, USAF, BSC
Chief, Optical Radiation Bioeffects Branch

MILLER.STEPHANIE.A.1230536283 Digitally signed by MILLER.STEPHANIE.A.1230536283 Date: 2024.02.03 13:01:43 -06'00'

STEPHANIE A. MILLER, DR-IV, DAF
Chief, Bioeffects Division
Airman Systems Directorate
711th Human Performance Wing
Air Force Research Laboratory

This report is published in the interest of scientific and technical information exchange, and its publication does not constitute an official position of the U.S. Government.

REPORT DOCUMENTATION PAGE

PLEASE DO NOT RETURN YOUR FORM TO THE ABOVE ORGANIZATION.

1. REPORT DATE	2. REPORT TYPE	3. DATES COVERED	
		START DATE	END DATE
18-NOV-2023	Interim / Final Report	JUN 2023	SEP 2023

4. TITLE AND SUBTITLE

Non-Fourier Laser-Tissue Heating Analysis: A Bio-heat Transfer Equation Comparison

5a. CONTRACT NUMBER	5b. GRANT NUMBER	5c. PROGRAM ELEMENT NUMBER
FA8650-19-C-6024		
5d. PROJECT NUMBER	**5e. TASK NUMBER**	**5f. WORK UNIT NUMBER**
		H17F

6. AUTHOR(S)

Sara Botelho-Andrade, Elharith M. Ahmed, Matthew G. Seman, Andrew W. Wharmby, Raniero A. Lara-Garduno

7. PERFORMING ORGANIZATION NAME(S) AND ADDRESS(ES)

Air Force Research Laboratory
711th Human Performance Wing
Human Effectiveness Directorate
Bioeffects Division
Optical Radiation Bioeffects Branch
4141 Petroleum Dr
JBSA Fort Sam Houston TX, 78234

SAIC, Inc.
4141 Petroleum Dr
JBSA Fort Sam Houston TX, 78234

8. PERFORMING ORGANIZATION REPORT NUMBER

9. SPONSORING/MONITORING AGENCY NAME(S) AND ADDRESS(ES)	10. SPONSOR/MONITOR'S ACRONYM(S)	11. SPONSOR/MONITOR'S REPORT NUMBER(S)
Air Force Research Laboratory 711th Human Performance Wing Human Effectiveness Directorate Bioeffects Division Optical Radiation Bioeffects Branch	711 HPW/RHDO	AFRL-RH-FS-TR-2024-0001

12. DISTRIBUTION/AVAILABILITY STATEMENT

DISTRIBUTION STATEMENT A. Approved for public release; distribution is unlimited. Cleared: AFRL PA Case Number: AFRL-2024-0698. The views expressed are those of the author and do not necessarily reflect the official policy or position of the Department of the Air Force, the Department of Defense, or the United States Government.

13. SUPPLEMENTARY NOTES

note

14. ABSTRACT

This study is aimed to examine limitations of the Fourier's law-based Pennes' bio-heat diffusion equation and the inclusion of a time-lag term to overcome those limitations. The estimates provided for the time-lag are based on available optical and thermal properties of the skin tissue. Contemporary methods used to model laser-tissue interactions most commonly employ Pennes' bio-heat equation. Despite its successful implementation in many applications, Pennes' equation reflects some unrealistic assumptions, such as the condition of infinite thermal propagation speed. While in many applications the effect of this assumption may be negligible, evidence shows that this assumption may produce unrealistic temperature profiles in extreme cases (such as laser heating applications) depending on the complexity of the tissue structure. To provide a theoretical framework, a linearized constitutive heat flux equation introduced by researchers in the 1960s is shown to unify the classical Pennes' bio-heat equation with the Thermal Wave Model for Bio-heat Transfer and some other alternative models. This perspective highlights the similarities and fundamental differences between the approaches. This report also aims to introduce and discuss the advantages and disadvantages of alternate models to correct these assumptions. A detailed overview of modern alternatives to Pennes' equation, including a numerical comparison between a thermal relaxation time method, the classical Pennes' bio-heat equation, and a fractional Pennes' equation, is provided.

15. SUBJECT TERMS

non-Fourier heat transfer, bio-heat equation, Pennes' equation, fractional models, thermal relaxation

16. SECURITY CLASSIFICATION OF:			17. LIMITATION OF ABSTRACT	18. NUMBER OF PAGES
a. REPORT	b. ABSTRACT	c. THIS PAGE		
U	U	U	U	35

19a. NAME OF RESPONSIBLE PERSON	19b. PHONE NUMBER *(include area code)*
Andrew Wharmby	(210) 539-8284

This Page Intentionally Left Blank

TABLE OF CONTENTS

LIST OF FIGURES

LIST OF TABLES

LIST OF EQUATIONS

1.0 SUMMARY

Contemporary methods used to model laser-tissue interactions most commonly employ Pennes' bioheat equation. Despite its successful implementation in many applications, Pennes' equation reflects some unrealistic assumptions, such as the condition of infinite thermal propagation speed. While in many applications the effect of this assumption may be negligible, evidence shows that this assumption may produce unrealistic temperature profiles in extreme cases (such as laser heating applications) depending on the complexity of the tissue structure. To provide a theoretical framework, a linearized constitutive heat flux equation introduced by researchers in the 1960s is shown to unify the classical Pennes' bio-heat equation with the Thermal Wave Model for Bioheat Transfer (TWMBT) and some other alternative models. This perspective highlights the similarities and fundamental differences between the approaches.

A detailed overview of modern alternatives to Pennes' equation, including a numerical comparison between a thermal relaxation time method, the classical Pennes' bioheat equation, and a fractional Pennes' equation, is provided. As a case study, limitations of the Fourier's law-based Pennes' bio-heat diffusion equation are examined and subsequently modified by including a time-lag term to overcome those limitations. The estimates provided for the time-lag are based on available optical and thermal properties of the skin tissue. It is postulated that a more accurate estimate of the time-lag can be achieved with improved characterization of the optical and thermal properties of the skin tissue and the temperature dependent protein unfolding and aggregation.

2.0 INTRODUCTION

At the time of writing, most standard methods used to model thermal damage from laser-tissue interactions rely on Fourier's law-based theories that implicitly assume an infinite thermal propagation speed. As a result, these models exhibit a temperature response that propagates instantaneously throughout the entire structure; a quality that is commonly non-physical due to thermal conduction being a mechanical phenomenon and therefore is transferred in solids with the velocity of sound. For cases with lower power and/or longer exposure durations, this assumption generally does not cause any problems. However, as the power is increased and the exposure duration reduced, this assumption tends to produce non-physical results. For example, while the implementation of the resulting bio-heat equation, known as Pennes' equation, has been generally successful in predicting temperature profiles for laser-tissue heating events, many times this is only achieved by varying tissue properties without full consideration of extraneous variables and sometimes assuming values that are outside the boundaries of known measurements [1].

Methods to obviate this problem include introducing a phase lag (or relaxation) term which accounts for a finite thermal propagation speed [2], [3]. This finite thermal propagation speed reflects the lag between the energy being deposited from the source (in this context, a laser) and the subsequent diffusion of said energy to the rest of the medium which yields a hyperbolic wave equation. However, this phase lag term, in many cases, has a value that is not explicitly defined or known. Nevertheless, the advantages are that (1) assuming a finite thermal propagation speed may account for the extreme conditions where Fourier's law begins to break down [4]–[6] and (2) the phase lag parameter can be used to intentionally account for variations in tissue properties.

This work details the investigation conducted on the inclusion of a phase lag term within the bio-heat equation and the physical as well as mathematical consequences for doing so. Requirements of the phase lag term as a physical parameter are also discussed along with possible approximation methods if the value itself cannot be determined experimentally. This work then concludes with a comparison study between the numerical implementation of governing equations with and without a phase lag term included in various contemporary models.

2.1 A linearized constitutive equation for heat conduction

The thermodynamic theory of materials with memory gained traction in the 1960s [7], [8]. Gurtin and Pipkin [9] developed a general theory of heat conduction for nonlinear materials with memory which captures finite propagation speeds. This work is based on the fading memory approach in the sense of Coleman and Noll [10]. The constitutive assumption of this work is that the response of the material at each point is characterized by functionals representing the present values of free energy $\psi = \psi(t)$, entropy $\eta = \eta(t)$, and the heat-flux $q = \mathbf{q}(t)$ at a point $\mathbf{x}$ whenever the present value of the temperature, the summed histories of temperature, and the gradient are known at $\mathbf{x}$. That is, $\psi(t) = \Psi(T, \overline{T}^t, \overline{\nabla T}^t)$, $\eta(t) = N(T, \overline{T}^t, \overline{\nabla T}^t)$, $\mathbf{q}(t) = Q(T, \overline{T}^t, \overline{\nabla T}^t)$ where Ψ, N, and Q represent the previously mentioned functionals and T repesents the temperature. The terms $\overline{T}^t$ and $\overline{\nabla T}^t$ represent the history functions and the notation is clarified in the next paragraph. In this context, a functional refers to a mapping from a space X into the field of real numbers. It should also be noted that this theory depends on the assumption that ψ, η, and q are independent of the present value of ∇T and for a theory in which the present value of ∇T is considered in the constitutive equation, see [11].

For the purpose of notation, if f is a function defined on $\mathbb{R}$, then f^t and $\bar{f}^t$ denote the history of f and the summed history of f up to time t. More explicitly, f^t and $\bar{f}^t$ are functions on $[0,\infty)$ defined by

$$\begin{aligned} f^t(s) &= f(t-s), \\ \bar{f}^t(s) &= \int_0^s f^t(\lambda)\, d\lambda = \int_{t-s}^t f(\tau)\, d\tau. \end{aligned} \tag{1}$$

Equation 1. History functions

The norm $\|f\|$ of a measurable scalar- or vector-valued function f on $[0,\infty)$ is defined as

$$\|f\|^2 = \int_0^\infty |f(s)|^2 h(s)\, ds, \tag{2}$$

Equation 2. Weighted L^p Norm

where h is a fixed influence function. That is, h is a continuous monotonically decreasing function such that $s^2 h(s)$ is integrable on $[0,\infty)$. Let H(or $\mathbf{H}$) denote the set of all measurable real-valued (or vector-valued) functions f on $[0,\infty)$ with $\|f\| < \infty$. The main result in [9] uses the functional for free energy to then determine the heat flux, which is necessary for deriving the constitutive equation discussed in this report. For further information on the function space and weights being

considered, please refer to Appendix A.

Theorem 1. *The response functional Ψ determines N through the entropy relation*

$$N = -D_T\Psi$$

and Q through the heat-flux relation

$$Q = -TJ_{\nabla T}\Psi.$$

Further, the dissipation inequality

$$J_T\Psi(T,\overline{T}^t,\overline{\nabla T}^t)T - \delta\Psi(T,\overline{T}^t,\overline{\nabla T}^t)(T^t,\nabla T^t) \leq 0$$

In the previous theorem, $D_T\Psi$ denotes the partial derivative with respect to T,

$$\delta\Psi(T,\overline{T}^t,\overline{\nabla T}^t)(T^t,\nabla T^t) = \delta_1\Psi(T,\overline{T}^t,\overline{\nabla T}^t)(T^t) + \delta_2\Psi(T,\overline{T}^t,\overline{\nabla T}^t)(\nabla T^t),$$

where δ_1 and δ_2 denote the partial (Fréchet) derivative with respect to $\overline{\theta}^t$ and $\overline{g}^t$ respectively (see A). And

$$J_T\Psi(T,\overline{T}^t,\overline{\nabla T}^t) = \delta_1\Psi(T,\overline{T}^t,\overline{\nabla T}^t)(1^c) \in \mathbb{R}$$
$$J_{\nabla T}\Psi(T,\overline{T}^t,\overline{\nabla T}^t)\cdot v = \delta_2\Psi(T,\overline{T}^t,\overline{\nabla T}^t)(\mathbf{v}^c) \in \mathbb{R}^3$$

for any $v \in \mathbb{R}^3$ where $1^c \in H$ and $\mathbf{v}^c \in \mathbf{H}$ are constant function with values 1 and $\mathbf{v}$, respectively. See Appendix A for more details.

This theorem is critical in deriving the representation of the heat flux term in the following equation [9].

$$\mathbf{q} = -\int_0^\infty a(s)\mathbf{g}(t-s)\,ds \tag{3}$$

Equation 3. Gurtin and Pipkin flux term

where $\mathbf{g}$ represents the temperature gradient ∇T. By varying the choice of the kernel $a(s)$, the flux terms for Pennes' equations (both the classical and fractional versions), the TWMBT, and the Type 1 Dual Phase Lag (DPL) Bio-heat model can be derived.

- Let $a(s) = \kappa\delta(s)$ then

$$\mathbf{q} = -\int_0^\infty \kappa\delta(t-s)\nabla T(s)\,ds = -\kappa\nabla T(t). \tag{4}$$

Equation 4. Fourier Law

This is the flux term used in Pennes' equation.

- Let $a(s) = \frac{\kappa}{\tau_q} e^{-\frac{t}{\tau_q}}$ then

$$\mathbf{q} = -\int_0^{\infty} \frac{\kappa}{\tau_q} e^{-\frac{(t-s)}{\tau_q}} \nabla T(s)\, ds. \tag{5}$$

Equation 5. Gurtin and Pipkin single phase lag

On the other hand, solving the first-order approximation of the single phase lag flux (equation 16) yields

$$\mathbf{q} = \mathbf{q}(r,0) e^{-\frac{t}{\tau_q}} - \int_0^{t} \frac{\kappa}{\tau_q} e^{-\frac{(t-s)}{\tau_q}} \nabla T(s)\, ds \tag{6}$$

Equation 6. Integral form of single phase lag

which equals equation (5) if $\mathbf{q}(r,0) = 0$. Likewise, if the magnitude of $e^{-\frac{t}{\tau_q}}$ is sufficiently small (e.g. if t is very large), this term may be negligible. This is the flux term used in the TWMBT.

Comparing equations (4) and (5) shows that in time space, the heat flux q is a point function of ∇T at time t in Fourier's law. The Cattaneo-Vernotte equation [2], [3] expresses q as a path function over the entire history (from $t = 0$ to t) during which ∇T is established. In [12], Liu notes that the heat flux q at time t in the TWMBT is respective to the value of q at time $t - t^*$, where t^* is the time for surface heat flux to travel to the specified point $\vec{r}$ and can be expressed as $t^* = \frac{|\vec{r}|}{C_t}$ and C_t represents the speed of the thermal wave in the tissue (or the "second sound"). Liu speculates that the difference between $\mathbf{q}(\vec{r},t)$ and $\mathbf{q}(\vec{r},t-t^*)$ causes the deviation between Pennes' equation and the TWMBT. Near the skin surface when $\vec{r} \to 0$, the two models predict similar values [12], [13] and the value of t^* is small enough to be negligible and $\mathbf{q}(\vec{r},t) - \mathbf{q}(\vec{r},t-t^*)$ is small.

In the early stage of external heating, it is possible for the tissue temperature to remain unchanged if most of the incident energy is consumed by the non-thermal biological activities (for example driving a water particle or an ion, changing electrical potential of cell membrane, or triggering a biochemical process). This is the temperature delay phenomenon observed in experiments using simple bologna meat with two phases of solid and water [4]. Wave-like conduction in the bologna was shown to be caused by the propagation of water by simulating the non-homogeneous biological material as a de-formable and two-phase porous medium [14]. In this case, the characteristic time can be theoretically estimated to be several seconds and the significance of this is that early external heating has been used to drive the water but not to increase the temperature of the solid phase.

- To try to identify the appropriate kernel for the flux in the Dual-Phase lag model we begin with the first-order approximation of the dual-phase lag flux term

$$\begin{aligned} \mathbf{q}(\vec{r},t+\tau_q) &= -k\nabla T(\vec{r},t+\tau_T) \\ \mathbf{q} + \tau_q \frac{\partial \mathbf{q}}{\partial t} &= -k\left[\nabla T + \tau_T \frac{\partial \nabla T}{\partial t}\right] \end{aligned} \tag{7}$$

Equation 7. Dual phase lag flux

Note that the difference between this flux term and the flux term used in the TWMBT is the introduction of a second relaxation term τ_T. Then the solution becomes

$$\mathbf{q} = \underbrace{e^{-\frac{t}{\tau_q}}\mathbf{q}(r,0) - \frac{\kappa}{\tau_q}\int_0^t e^{-\frac{(t-s)}{\tau_q}}\nabla T(r,s)\,ds}_{\text{Single Phase Lag Term}} - \underbrace{\frac{\kappa\tau_T}{\tau_q}\nabla T(r,t)}_{\text{Fourier-type Term}} + \frac{\kappa\tau_t}{\tau_q}e^{-\frac{t}{\tau_q}}\nabla T(r,0) + \frac{\kappa\tau_T}{\tau_q^2}\int_0^t e^{-\frac{(t-s)}{\tau_q}}\nabla T(r,s)\,ds \tag{8}$$

Equation 8. Dual phase lag flux integral from

In the context of the previously discussed models, this flux term is a linear combination of the previous flux terms. In this perspective, the modification to the Fourier-type term would be $\left(\frac{\kappa\tau_t}{\tau_q}e^{-\frac{t}{\tau_q}} - \frac{\kappa\tau_T}{\tau_q}\nabla T(r,t)\right)$.

It should be remarked that the Gurtin and Pipkin constitutive equation is a particular case of the fading memory concept. The fading memory concept relates the flux $j(x,t)$ to its gradient using the Boltzmann linear superposition functional to express the flux history [15] through the influence of the memory kernel R. In the following equations, D_0 and D' are transport coefficients and $C(x,t)$ is a causal function (which vanishes for $t < 0$). Two popular uses of this concept in the bioheat application are:

1. For simple fading memory (SFM) the heat flux is represented as

$$\nabla \cdot j(x,t) = -D'\int_0^t R(t-\tau)\nabla C(x,\tau)\,d\tau. \tag{9}$$

Equation 9. Simple fading memory concept

2. For extended fading memory (EFM) the heat flux is represented as

$$\nabla \cdot j(x,t) = -D_0\nabla C(x,t) - D'\int_0^t R(t-\tau)\nabla C(x,\tau)\,d\tau. \tag{10}$$

Equation 10. Extended fading memory concept

Note that equation (9) comes from equation (10) for $D_0 = 0$.

In this context, fractional models such as the example proposed by Ferras et al. [16] employ the fading memory concept in which a simple power-law kernel is considered:

$$R(x,t) = \frac{t^{\alpha-1}}{\Gamma(\alpha)}, \qquad 0 < \alpha < 1. \tag{11}$$

Equation 11. Simple power law kernel

Following this idea, Hristov noted some discrepancies in the constitutive equation proposed by Ferras' et al. [16], [17] and cautions readers further investigation is needed to apply these

techniques in the specific case of bioheat models. However, adapting an approach of Joseph and Preziosi [18], Hristov proposed the following extended kernel:

$$R_{EPL}(x,t) = \kappa_1 \delta(t) + \kappa_2 \frac{t^{\alpha-1}}{\Gamma(\alpha)}, \qquad 0 < \alpha < 1. \tag{12}$$

Equation 12. Extended power law kernel

Joseph and Preziosi [18] considered a modified relaxation function consisting of two terms where the first term models the instantaneous (memory-less) reaction of the heat conductor and the second term captures the flux dampening effect and finite speed of propagation shown as

$$R_{JP}(x,t) = \kappa_1 \delta(t) + \frac{\kappa_2}{\tau} e^{-\frac{t}{\tau}}, \tag{13}$$

Equation 13. Joseph and Preziosi memory kernel

where κ_1 and κ_2 are the effective thermal conductivity and the elastic conductivity, respectively. Using this assumption in the conservation energy equation yields an integro-differential equation which contains both Fourier-like terms and non-Fourier terms [19]. The non-Fourier terms go to zero for large values of time since the memory function fades, however, the presence of the time variable in the second term is related to the assumption of finite heat flux speed [17]. This idea is an example of the extended fading memory concept using a simple exponential kernel.

Similar to equation (13), the use of the extended power law kernel yields an integro-differential equation whose second term represents the Riemann-Liouville fractional integral [20]. This observation coincides with results obtained by the extended fading memory concept and simple power-law kernel [17].

2.2 Influence of τ_q

In 1963, Marvin Chester introduced an analog of the second sound in helium II for solids [21], [22]. Working with dielectric solids, Chester determined a critical frequency for thermal fluctuations above which heat transport proceeds by wave propagation rather than diffusion. The idea that second sound exists in solids was noted by Ward and Wilks [23] and speculated by Peshkov [24] since its appearance depends only upon the presence of a phonon gas. Chester considered the continuity equation for heat transport without density or pressure gradients, given by

$$C\frac{\partial T}{\partial t} + \nabla \cdot q = 0, \tag{14}$$

Equation 14. Simplified Heat Equation

where C is the heat capacity per unit volume, $T = T(\vec{r},t)$ is the absolute temperature, and q is the thermal heat current density. Combining this equation with Fourier's law of thermal conductivity for heat flow produces the diffusion equation

$$\mathbf{q}(\vec{r},t) = -\kappa \nabla T(\vec{r},t), \tag{15}$$

Equation 15. Fourier conduction term

where κ is thermal conductivity and $\mathbf{q}(\vec{r},t)$ represents the heat flux at position $\vec{r}$.

As has been pointed out by many authors, the diffusion equation leads to an infinite propagation velocity for a finite thermal pulse [2], [3], [25]. To overcome this dilemma, Cattaneo introduced the thermal relaxation characteristic time τ_q, which is interpreted as "the time lag required to establish steady heat conduction in a volume element once a temperature gradient has been imposed across it" [26]. In other words, τ_q is the time needed to reach thermodynamic stability. Therefore, the relaxation time introduces the idea of a finite speed of heat propagation. The equation proposed by Cattaneo [2] (and separately by Vernott [3]) is

$$\mathbf{q}(\vec{r},t) + \tau_q \frac{\partial \mathbf{q}(\vec{r},t)}{\partial t} = -\kappa \nabla T(\vec{r},t), \qquad \tau_q > 0, \tag{16}$$

Equation 16. Modified unsteady heat conduction term

where the new term is called *thermal inertia* [27]. $\tau_q = \frac{\alpha}{C_t^2}$ is often referred to as the *thermal relaxation time*, where α is the thermal diffusivity and C_t is the speed of the thermal wave in the medium [4], [28]. The reciprocal of the relaxation time, $\frac{1}{\tau_q} = f$ is the critical frequency dictating the activation of thermal wave behavior [22].

The introduction of τ_q in the equation for heat flux yields an equation of hyperbolic type which characterizes the combined diffusion and wave-like behavior of heat conduction. The physical significance of equation (16) (or Cattaneo-Vernotte equation) is that there is finite build-up time for the onset of a thermal current after a temperature gradient is applied. The heat flow grows gradually with a relaxation time τ_q. When the thermal gradient is suddenly removed, there is a lag in the disappearance of the current which is captured in equation (16), but not in Fourier's law or equation (15). Considering equation (16) and the heat equation, a temperature T is produced which obeys a dissipative wave equation.

Based on equation (16) and the general bio-heat equation, a general form of the Thermal Wave Model of Bio-heat Transfer (TWMBT) in living tissues was initially introduced by Liu *et al.* [29].

$$\begin{aligned} \nabla \cdot [\kappa \nabla T(\vec{r},t)] + \omega_b c_b (T_b - T) + q_m + q_s + \tau_q \left(-\omega_b c_b \frac{\partial T}{\partial t} + \frac{\partial q_m}{\partial t} + \frac{\partial q_s}{\partial t} \right) \\ = \rho c \left[\tau_q \frac{\partial^2 T}{\partial t^2} + \frac{\partial T}{\partial t} \right] \end{aligned} \tag{17}$$

Equation 17. Thermal Wave Mode for Bio-heat Transfer

where T_b is the temperature of the perfused blood, ρ is the tissue density, κ is the thermal conductivity, c is the specific heat of the tissue, and ω_b represents the blood perfusion rate

coefficient. c_b is the specific heat of blood. q_m and q_s are volumetric heat due to metabolism and spatial heating, respectively. This equation is numerically implemented and compared to Pennes' bio-heat equation in section 3.

The relaxation time τ_q (sometimes referred to as the phase lag) is associated with the communication time between phonons (or phonon-phonon collisions) for the commencement of the resistive flow [30], [31]. In fact, τ_q is described as the time for the establishment of a resistive flow [22] and the rate $\frac{1}{\tau_q}$ refers to the frequency of collisions of a lossful nature (i.e. those which give rise to a thermal resistance). For this reason, τ_q is expected to be proportional to κ [22]. If R is considered to represent the total collision rate, then R encompasses all types of collisions including lossless collisions (which do not give rise directly to thermal resistance). For this reason, R is expected to be higher than $\frac{1}{\tau_q}$ and it establishes an upper frequency f_r (for phonon-distribution fluctuations) above which the concept of temperature loses its meaning. The thermal equilibrating rate is of order R which means that $\frac{1}{R}$ is the time necessary to establish the local thermal equilibrium and this time is less than τ_q (or the time to establish steady-state resistive flow) [22].

Estimating τ_q correctly is important because it determines the critical frequency and the attenuation of the thermal wave. Chester's attempt to evaluate τ_q quantitatively relies on the physical grounds that the square of the thermal wave propagation velocity v is one third of the square of the phonon velocity, s, or $v^2 = \frac{1}{3}s^2$ [22].

The previous equation is assumed to hold for mediums in which the transport of heat occurs via the phonon gas. The basis for this comes from the assumption that the thermal wave constitutes a coherent propagation of density disturbances in the phonon gas.

Considering the heat flux relationship given in equation (16) and the simplified heat equation (14), then the resulting equation predicts a finite upper-limiting velocity for the propagation of a thermal signal v given by $v^2 = \frac{\kappa}{\tau_q C}$ [22]. An aspect of interest of this occurs in the high frequency limit of fast-thermal fluctuations. If T varies at a rate $f = \frac{1}{2\pi}\frac{1}{T}\frac{\partial T}{\partial t}$, which is much faster than $f_c = \frac{1}{2\pi\tau_q}$, then the resulting equation predicts wave propagation of temperature instead of diffusion [22]. The frequency f_c is the critical frequency for the onset of thermal waves and this frequency is directly proportional to the thermal resistivity.

Recall that the Cattaneo-Vernott constitutive relation [2], [3] is actually a first-order approximation of a more general constitutive relation

$$\mathbf{q}(\vec{r}, t+\tau_q) = -\kappa \nabla T(\vec{r}, t). \tag{18}$$

Equation 18. Single phase lag flux

which shows that the temperature gradient established at a point $\vec{r}$ at time t gives rise to a heat flux vector at $\vec{r}$ at a later time $t+\tau_q$. There is a finite build-up time τ_q for the onset of heat flux at $\vec{r}$ after a temperature gradient is applied. This is why τ_q is described as the time lag needed to establish the heat flux when a temperature gradient is applied. The impact of the second-order derivative term $\tau_q \frac{\partial^2 T}{\partial t^2}$ in the hyperbolic heat-conduction equation is determined by three factors: the value of

τ_q, the value of $\frac{\partial T}{\partial t}$, and the time scale involved.

The value of τ_q is material-dependent [28]. For most solid materials τ_q varies from 10^{-10} s to 10^{-14} s and for most gases the range is 10^{-8} s $\sim 10^{-10}$ s [32]. In biological materials and materials with non-homogeneous inner structures, the value of τ_q have been observed to be up to 10^2 s [4], [33]–[36]. This suggests that the thermal relaxation effects can be important even in common engineering applications where the time scales of interest are of the order of a fraction of a minute. The wave nature of a thermal signal will dominate the diffusive behavior when [37]

$$\frac{\partial T}{\partial t} >> \frac{T_r}{2\tau_q} e^{\frac{t}{\tau_q}},$$

where T_r is the reference temperature. This inequality suggests that the wave-like features will become significant when τ_q is large, $\frac{\partial T}{\partial t}$ is large, or t is small.

To better understand the high magnitude of the characteristic time in living tissues, Liu [12] proposed a new conceptual equation to correlate the heat flux with the temperature gradient. Liu [12] suggested that the actual flux used to establish a temperature gradient is actually different from the flux q that is originally applied. That is, part of the flux will be absorbed to drive the mechanical, electrical, and chemical processes. This flux that is induced by the heat transport, but does not appear in the form of heat, is defined as the converted energy flux $\mathbf{q}_{\text{con}}$:

$$\begin{aligned} \mathbf{q}(\vec{r},t+\tau_q) - \mathbf{q}_{\text{con}}(\vec{r},t) &= -\kappa \nabla T(\vec{r},t), \\ \mathbf{q}(\vec{r},t) + \tau_q \frac{\partial \mathbf{q}(\vec{r},t)}{\partial t} - \mathbf{q}_{\text{con}}(\vec{r},t) &= -\kappa \nabla T(\vec{r},t), \end{aligned} \tag{19}$$

Equation 19. Modified single phase lag flux with energy conversion

where $\mathbf{q}_{\text{con}}$ is the converted energy flux given by the sum of mechanical, electrical, and chemical flux or $\mathbf{q}_{\text{con}}(\vec{r},t) = J_m(\vec{r},t) + J_e(\vec{r},t) + J_c(\vec{r},t)$. The second line in equation (19) uses the first-order approximation of the heat-flux and is typically used because it has been shown to be consistent with the second law of thermodynamics [38]–[40]. It is assumed that q_{con} and the temperature gradient ∇T occur simultaneously. Rewriting equation (19) then gives

$$\tau_q = \frac{\mathbf{q}_{\text{con}}(\vec{r},t) - \mathbf{q}(\vec{r},t) - \kappa \nabla T(\vec{r},t)}{\frac{\partial \mathbf{q}(\vec{r},t)}{\partial t}}. \tag{20}$$

Equation 20. Phase lag term representation

Determining the converted flux $\mathbf{q}_{\text{con}}$ is difficult without more information on how the specified energy activity takes place, but the concept of conversion efficiency (η) was applied to express the heat flux as $\mathbf{q}_{\text{con}}(\vec{r},t) = \eta \mathbf{q}(\vec{r},t)$. A method for calculating the conversion efficiency considering a coupling process in a two-mode energy system is available in [12].

In homogeneous materials, the electrons and phonons dominate the heat conduction and q_{con}

should be nearly zero [41]. In this case, the difference between $\mathbf{q}(\vec{r},t)$ and $\kappa\nabla T$ is extremely small (and so is τ_q) which is expected since in Fourier's law the difference is zero. However, for non-homogeneous materials, especially living tissue, there is a large q_{con} for mechanical, electrical, and chemical activities. q_{con} can have significant contributions to the value of the characteristic time, even for a small difference of $\mathbf{q}(\vec{r},t)$ and $\kappa\nabla T$, because $\frac{\partial \mathbf{q}(\vec{r},t)}{\partial t}$ is often small for bio-heat processes and q_{con} is possibly much larger than $-\mathbf{q}(\vec{r},t) - \kappa\nabla T$ in equation (20). For multi-mode energy couplings, such as in living systems, the external heating can be viewed as a force to trigger specific processes and the overall characteristic time τ_q is the combined effect of different energy conversions [12].

3.0 COMPUTATIONAL IMPLEMENTATION AND PERFORMANCE

Laser injury threshold is expressed as the energy or irradiance level required to produce a Minimum Visible Lesion (MVL). Typical laser-tissue interaction models accounts for optical energy deposition and subsequent heat transfer. Accurate modeling of the laser-induced thermal effect on biological tissue therefore hinges on the accuracy of the laser propagation model, heat transfer model, and how the optical and thermal properties are treated in the simulation. The current effort employed Beer's law and optical and thermal properties from Delisi et al. [42] listed in Table 1. Since hair follicles in shaved skin function as heat sources in ranges of 1070 nm and above [42], this analysis is limited to waxed skin data cases for accurate MVL estimates. Heat transfer is typically modeled by the Pennes bio-heat diffusion equation, which implies an infinite thermal propagation speed. The focus of this investigation is to demonstrate the capability of the TWMBT to model heat transfer in biological tissues, equation 17, as an alternative to the bio-heat diffusion equation when the assumption of an infinite thermal propagation speed is no longer valid. For the purpose of this analysis, a 2D system in cylindrical coordinates is being considered. Neumann boundary conditions (convective, evaporative, and radiative) are applied at the surface, a 1-D solution of the TWMBT (T [0, z] = T [z]) is being maintained at the beam axis boundary, and the background temperature (T_b) is being upheld at the other two boundaries of the solution domain (T [a, z] = T [b, z] = T_b).

In this analysis, the 1070 nm laser-induced thermal response predicted by the TWMBT model at the surface of the skin for exposure durations 0.01 s, 0.1 s, and 10 s are examined. To predict the thermal response resulting from exposure, the TWMBT approach uses the characteristic time (see section 2.2) to account for the time needed to accumulate sufficient localized thermal energy to prompt the diffusion process, an aspect that is not captured by the traditional bio-heat diffusion model. Using empirical data as the input for the TWMBT model, an optimized characteristic time for each exposure is calculated. This was achieved by varying the characteristic time and using a least-squared optimization method to establish the best possible approximation of the empirical temperature profile. The broad distribution of the characteristic times for a given exposure is attributed to the wide range of variability in biological tissues. As shown in Figure 1, a best-fit equation relating the characteristic time to laser power can be established after the elimination of outliers. Given the best fit equation, the characteristic time for a given threshold exposure can be predicted. Figure 1 shows calculated characteristic time and linear fits for 0.01 s, 0.1 s, and 10 s exposure duration. Using the characteristic time fits, the characteristic time for 0.01 s, 0.1 s, and 10 s threshold exposures are projected and a trend of the characteristic time as a function of exposure

duration is established (see Figure 2).

Table 1. Summary of optical, physical, and thermal properties used in the analysis

Property	Units	Layer	Value
Thickness	mm	Epidermis	0.082
		Dermis	2.7
		Fat	15
Optical absorption	cm^{-1}	Epidermis	0.35
		Dermis	0.17
		Fat	1.03
Reduced scattering	cm^{-1}	Epidermis	17.4
		Dermis	15.4
		Fat	8.94
Specific heat	$\frac{J}{kg \cdot K}$	Epidermis	2244
		Dermis	3663
		Fat	2070
Conductivity	$\frac{W}{m \cdot K}$	Epidermis	0.2
		Dermis	0.49
		Fat	0.16

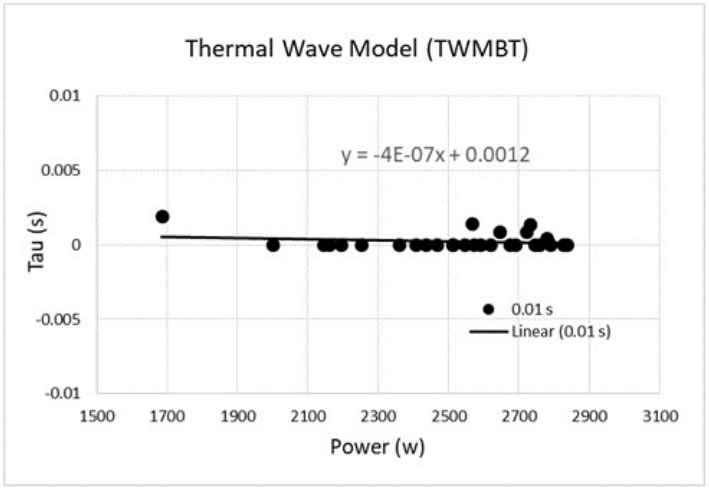

(a) 0.01 s exposure duration

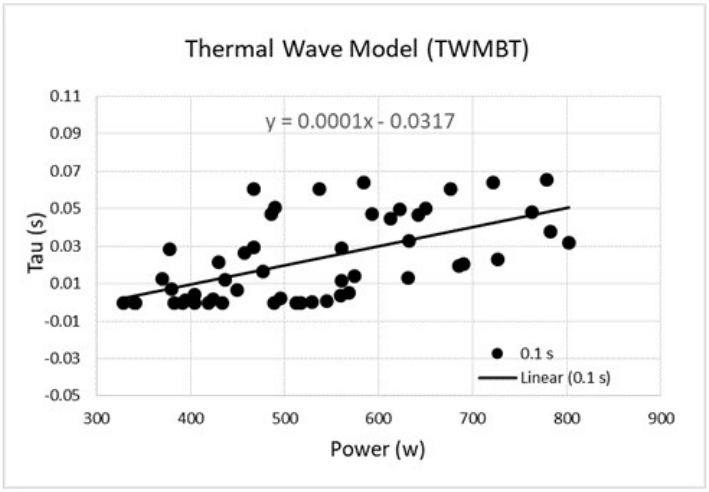

(b) 0.1 s exposure duration

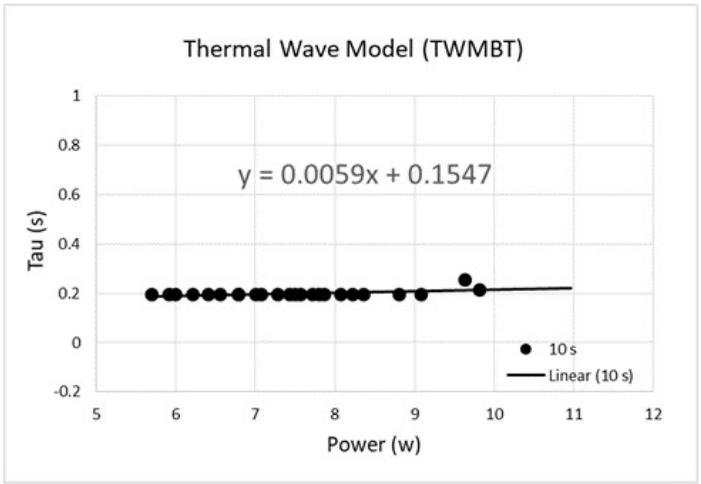

(c) 10 s exposure duration

Figure 1. Calculated characteristic time as a function of power with a linear fit for (a) 0.01 s, (b) 0.1 s, and (c) 10 s single pulse laser exposure to waxed porcine skin.

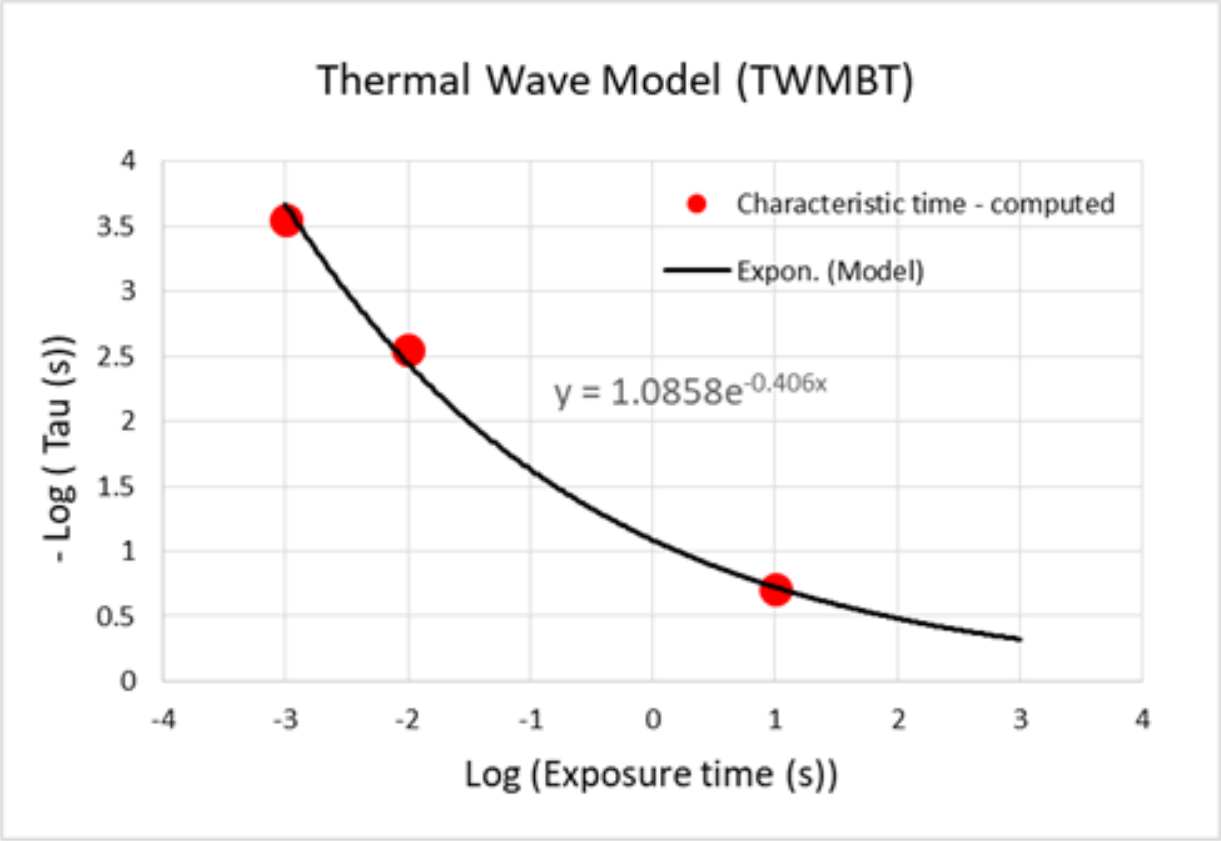

Figure 2. Characteristic time as a function of exposure duration.

Preliminary evaluation of the observed temperature rise for exposure durations 0.01 s and 0.1 s dictated the need to construct a new trend for the optical and thermal properties to simulate the skin interaction with the 1070 nm laser. Based on presently used absorption coefficient for the epidermis layer of 0.35 cm^{-1}, a conservative estimate of the peak temperature rise on the surface of the skin for 2780 W and 0.01 s exposure, assuming no heat loss to surrounding locations, is 8.5 °C. As reported by Delisi et al. [42], the expected peak temperature is 67.2 °C whereas the Scalable Effects Simulation Environment (SESE) predicted peak temperature is 65.0 °C. With an absorption coefficient of 0.35 cm^{-1} and a 379 W laser at an exposure of 0.1 s, the conservative estimate of the peak temp rise of 10.5 °C differed significantly from the observed temperature rise from 32 °C. Given the very low absorption coefficient of the dermis layer of 0.17 cm^{-1} as well as the very short exposure duration, this significant difference based on the assumed absorption coefficient and heat capacity is problematic to account for by heat diffusion from the hypodermis layer alone, as doing so would cause damage to the dermis layer. The very low absorption coefficient of the epidermis layer is believed to account for the poor estimate of peak temperature rise. A first attempt to bridge the gap between observed peak temperature rise and TWMBT model predictions was swapping the constant absorption coefficient of the epidermis layer with a dynamic absorption coefficient in the form of a hyperbolic tangent function (see equation 21). This choice permits a dynamic temperature-dependent absorption coefficient which accounts for the thermal energy required

for the observed peak temperature rise but it also simultaneously revealed a discrepancy in the temperature profile for the exposure durations of 0.01 s and 0.1 s as seen in Figure 3. Furthermore, the hyperbolic tangent function is a reasonable choice because it is a bounded increasing function, in particular equation 21 allows for an absorption coefficient that varies between approximately 0.26 and 1.78.

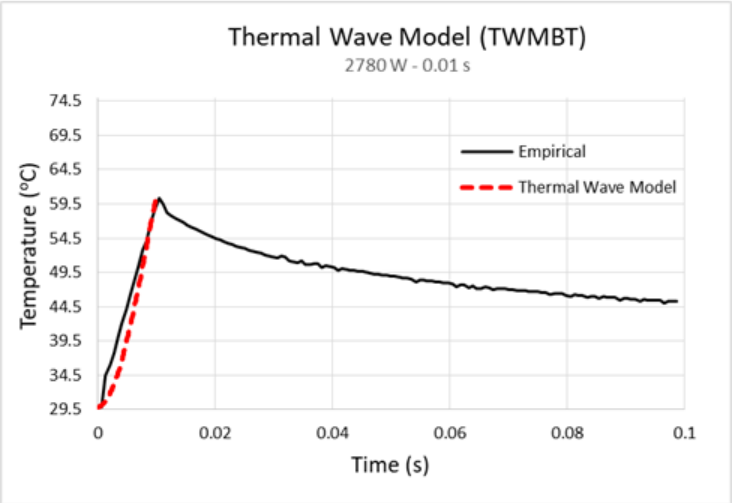

(a) 0.01 s exposure duration

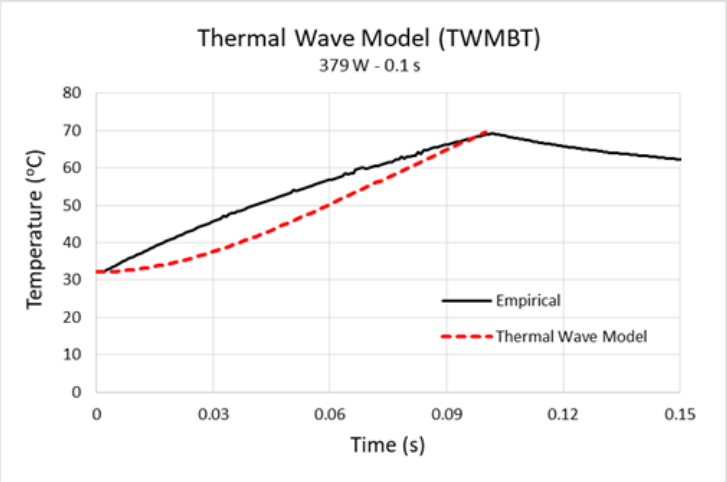

(b) 0.1 s exposure duration

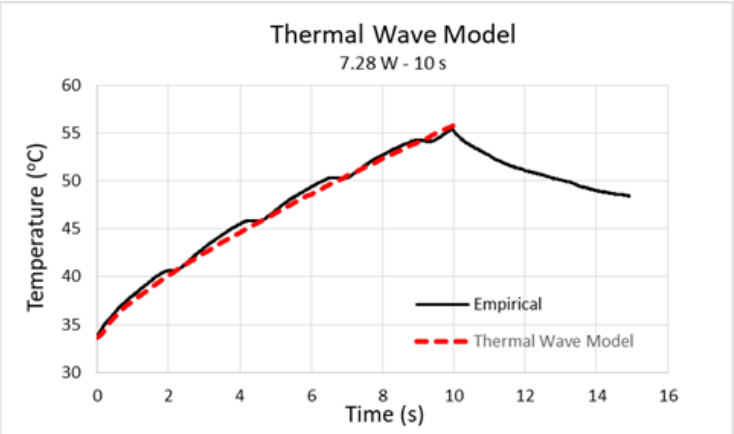

(c) 10 s exposure duration

Figure 3. Model and increasing temperature data for temperature-dependent absorption coefficient.

$$\alpha_{Epidermis}(T) = 0.998 - 0.782\tanh(7.74 - 0.32T) \tag{21}$$

Equation 21. Optical absorption coefficient of the epidermis layer

The discrepancy in the temperature profiles starting to surge at the very beginning of the exposure for the 0.01 s and 0.1 s duration cases can be attributed to the absorption coefficient, heat capacity, or both. Since the dynamic absorption coefficient described previously was formulated by taking into account a wide range of reported empirical absorption coefficients for the epidermis layer (0.35 cm^{-1} - 1.4 cm^{-1}), an adjustment to the specific heat trend is needed to compensate for the difference between predicted temporal temperature rise and the empirical temperature profile. A revised trend for the epidermis layer specific heat $C_{\text{Epidermis}}(T)$ was made by starting at a lower value which linearly rises with temperature (22). This appears to satisfy the desired thermal energy to predict the temporal temperature rise and the final peak temperature at the end of exposure. However, research indicates that the specific heat (as a function of temperature) is not a purely increasing function and researchers have found evidence that suggests some endothermic transitions are due to protein denaturation [43]. In fact, results in [43] suggest that the specific heat peaks in the approximate 50°C - 60°C range and then begins to decrease. Improving upon the accuracy of the specific heat term would improve characteristic time estimates and overall model accuracy.

$$C_{\text{Epidermis}}(T) = 26.32 \cdot T + 2044 \tag{22}$$

Equation 22. Specific heat of the epidermis layer

As shown in Fig 4, using the revised absorption coefficient and specific heat for the epidermis layer, the TWMBT model predicts the anticipated temperature profiles across exposure durations from 0.01 s to 10 s.

The laser injury threshold identified as the effective dose required for 50% probability of damage (ED50) is determined with the probit method. As reported by Delisi et al. [42], the 24 hr damage thresholds for exposure durations of 0.01 s, 0.1 s, and 10 s are 2300 W, 345 W, and 6.39 W respectively. Represented in figure 5 (a), (b), and (c) are experimental data for peak temperature against power. An estimate of the peak temperature for exposure can be extracted from the empirical thermal profiles provided. Exposure that resulted in 24 hr damage is shown in red while no damage is shown in black. Given the ED50 values for exposure durations of 0.01 s, 0.1 s, and 10 s displayed in the figures with the red vertical dashed lines, an estimate of the peak temperature rise for each threshold exposure is displayed with a red horizontal dashed line.

TWMBT threshold predictions were compared with SESE predictions for 0.01 s, 0.1 s, and 10 s exposure durations. As shown in figure 6, a relatively good level of agreement between the models is observed for the threshold exposures of 2780 W, 379 W, and 7.28 W. It is important to note that the SESE prediction is lower compared to that of the TWMBT model for the 10 s exposure duration. The difference in peak temperature rise is reduced with an increase in exposure duration, and SESE's predicted temperature rise exceeded the TWMBT predictions at 0.01 s. This trend of a shift in peak temperature is the result of a combination of differences in the absorption coefficient

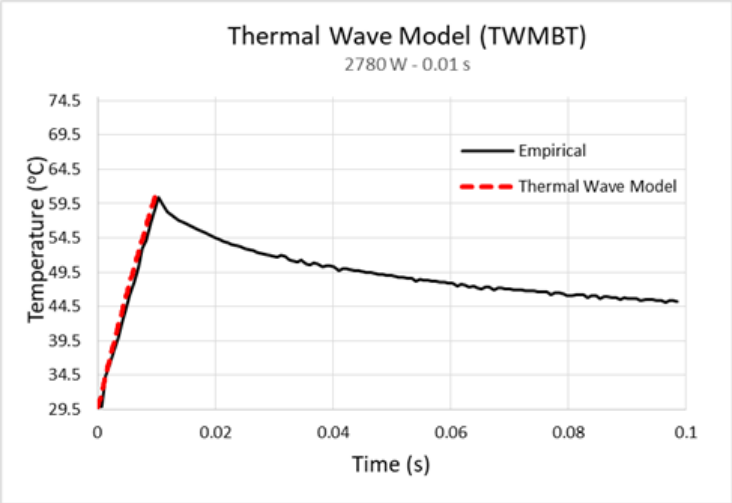

(a) 0.01 s exposure duration

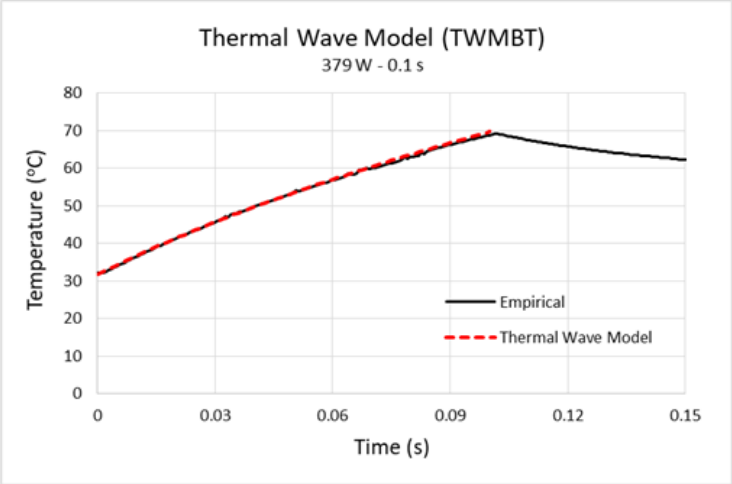

(b) 0.1 s exposure duration

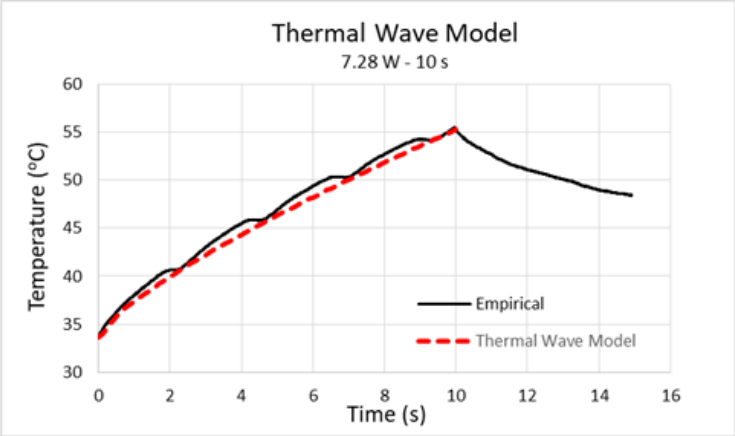

(c) 10 s exposure duration

Figure 4. Model and increasing temperature data for temperature-dependent absorption coefficient and specific heat.

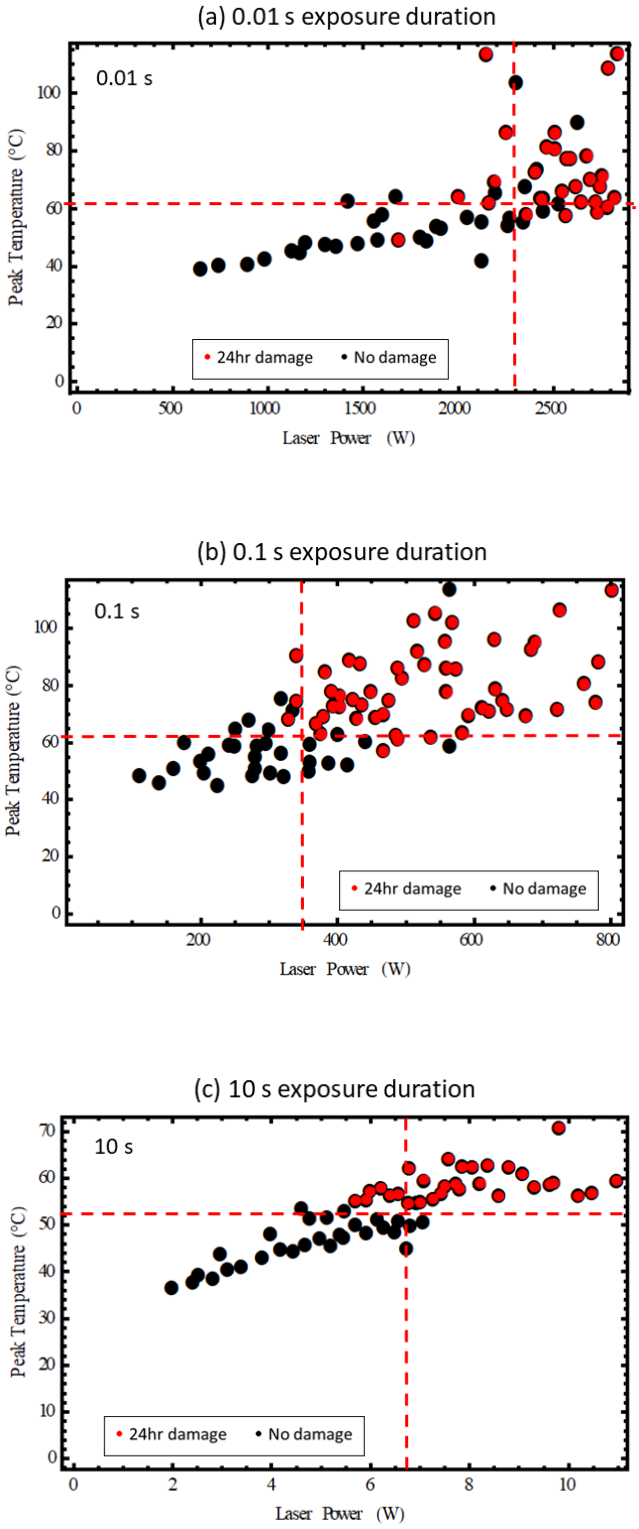

Figure 5. Peak temperature as a function of power with vertical and horizontal dashed red lines for empirical laser power threshold exposure and estimate for mean temperature threshold, respectively.

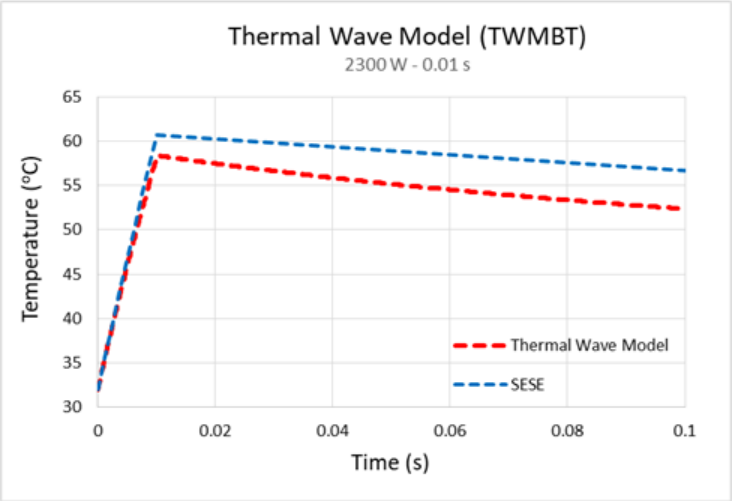

(a) 0.01 s exposure duration

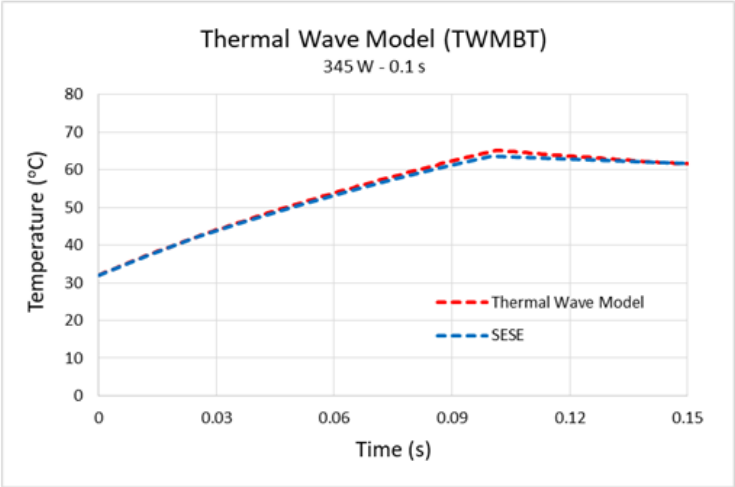

(b) 0.1 s exposure duration

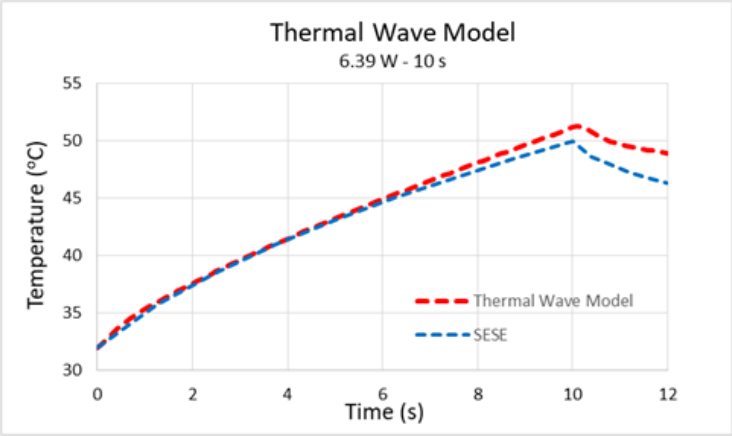

(c) 10 s exposure duration

Figure 6. Comparison SESE using SESE's dynamic skin model and TWMBT with temperature-dependent absorption coefficient and specific heat.

and heat capacity estimate used in the two models. The temperature profile predicted by SESE is crafted using a temperature-dependent heat capacity profile for the epidermis layer that is concave up with a minima around 40 $^{\circ}C$.

As shown in figure 7, SESE's most accurate approach to predict threshold exposure effects loses accuracy as the exposure level shifts away from the damage threshold for exposure duration 0.01 s, 0.1 s, and 10 s. It is also important to note that the TWMBT model maintained an accurate prediction of temperature rise while shifting away from damage threshold exposure. This result, shown in figures 6 and 7, is also a confirmation that the TWMBT approach is equipped with the tools needed to predict tissue thermal response as a function of power and exposure duration. Since the focus of this analysis was to simulate the skin thermal response while it is being exposed to the laser, issues connected to post exposure profile seen in the TWMBT generated results is attributed to thermal properties used in the simulation and remain to be investigated and modeled correctly and are considered to be beyond the scope of this effort.

For these experiments the thermal wave model was implemented across a 2D spatial and 1D temporal domain consisting of (100 X 100 X 200) cells. Energy transport across these cells is performed by an approximation of cell absorption through Beer's Law. In contrast, SESE models were implemented across a 3D spatial and 1D temporal domain consisting of (14 X 150 X 150 X 400) cells. SESE determines energy transfer through the radiative transfer model which is solved using Monte Carlo simulations [44]. Despite calculation and domain differences between the models, a naive comparison between their computational complexities can be drawn by determining the amount of cells each simulation calculates within a given simulation time. A definite comparison between these models cannot be concluded on without expanding the thermal wave model into a 3D spatial dimensions and matching simulation domains. The interaction of cells across another spatial dimension will almost certainly increase the computation time for the thermal wave model, but cost may also be reduced in calculating radiation absorption compared to SESE due to it being approximated through Beer's Law rather than using the radiative transport model. These results are shown in table 2 for each exposure duration of interest used in this study.

Table 2. Computational complexity comparison between Thermal Wave Model and SESE

Model	Exposure Duration (s)	Simulation Time (s)	Cells Modeled	Cells/s
SESE	0.01	872.732	126000000	144374
TWM	0.01	7.029	9000000	1280409
SESE	0.1	1088.206	126000000	115786
TWM	0.1	7.066	9000000	1273705
SESE	10	2069.275	126000000	60890
TWM	10	6.987	9000000	1288106

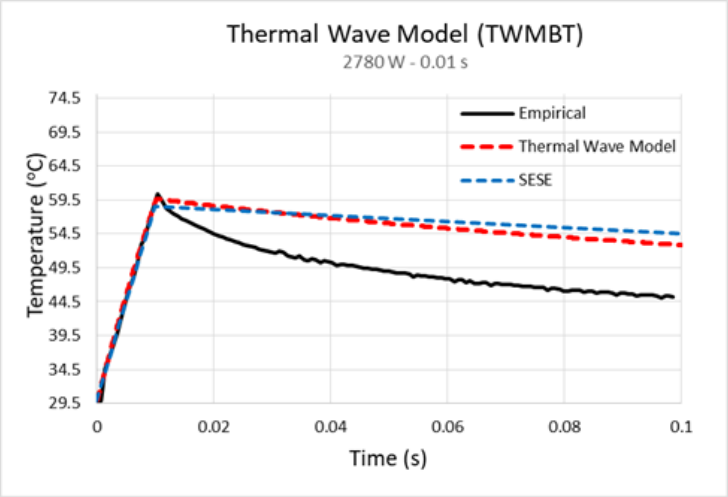

(a) 0.01 s exposure duration

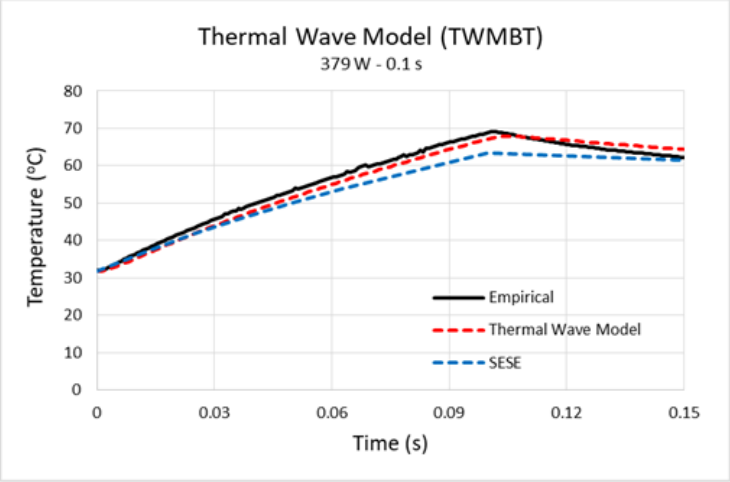

(b) 0.1 s exposure duration

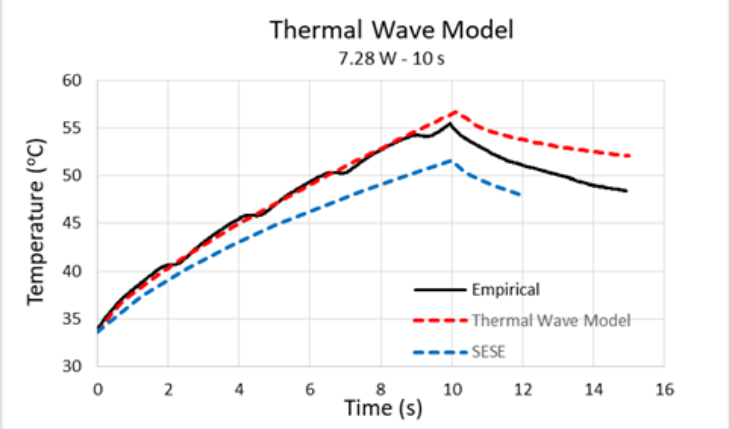

(c) 10 s exposure duration

Figure 7. Comparison of empirical damage threshold data, SESE, and TWMBT.

4.0 CONCLUSIONS

This effort investigated the limitations of the Fourier's law-based Pennes' bio-heat diffusion equation and examined the inclusion of a phase lag term as an option for a more robust physics-based modeling approach to simulate laser tissue interaction. In addition, a constitutive equation for heat flux was investigated to provide a theoretical framework that unifies the models discussed in [1] and provides context for the phase lag term used in the TWMBT. The Pennes' bio-heat equation is based on the Fourier assumption that the heat flow is directly proportionate to the gradient of the temperature which results in an infinite thermal propagation speed. This is unrealistic in many real-world applications and has been questioned by various authors [4], [37], [45]. It was found that the success of this approach in predicting laser induced thermal effect relies on varying the tissue optical and thermal properties. Additionally, this approach often results in a wide range of values for the tissue absorption coefficient and specific heat which are used to achieve an acceptable tissue response for varying exposures. Introducing the phase lag to the heat diffusion equation (in the form of a characteristic time) provides a framework to account for a finite thermal propagation speed resulting in a thermal wave. This approach takes into account contributions from the time rate of change for the internal and external heat sources as well as the acceleration of the temperature rise during the exposure. Since the characteristic time is a measure of the time needed to reach thermodynamic stability, it is a material-specific quantity and changes as a function of rate of temperature rise. An estimate of the characteristic time for biological tissues (non-homogeneous structures) requires knowledge of the thermal resistivity of the medium and the critical frequency for the onset of the thermal wave. Thus, there is no simple function that provides an estimate of the characteristic time taking into account the complexity of the medium and the rate of temperature rise (non-isothermic process). Therefore, characteristic time estimates provided in this investigation are based on available optical and thermal properties of the skin tissue layers (see Figure 1). Improved estimates of the characteristic time are attainable with accurate modeling of the skin tissue optical and thermal properties, such as the optical absorption coefficient of the epidermis layer $\alpha_{\text{Epidermis}}(T)$ and specific heat $C_{\text{Epidermis}}(T)$. Experiments which allow heat conduction to be the dominant heat transport mechanism, as opposed to other heat source and heat generation mechanisms, will be easier to determine whether a non-Fourier phenomenon is observed or not. In this case, the measurements are less likely to be misinterpreted and the non-Fourier parameters are easier to determine. This can be difficult, since volumetric heat generation is inevitable in many practical situations and it could dominate the time evolution of the temperature field.

It is also important to note that exposure to laser radiation leads to a temperature increase of the cell, protein denaturation, and other effects. Protein denaturation accounts for a significant share of the deposited thermal energy and manifest as an increase in specific heat [43], [46]. Only a portion of the deposited thermal energy is used by the living cell to drive the temperature rise. Therefore, accurate modeling of tissue dynamic properties is vital for accurate assessment of the tissue thermal response. Since denatured protein is a leading contributor to cell death [43], [46], quantifying the temperature induced denaturation of protein is of a great importance. Additional efforts to characterize the unfolding of protein and its dependence on temperature will result in an increased accuracy of the characteristic time estimate provided in this study. Incorporation of all of the aforementioned protein characteristics and their respective effects on the overall temperature

profile and peak temperature reached during an exposure would also greatly increase the accuracy and, in turn, the overall validity of the models discussed in this work that assume a finite thermal propagation speed rather than infinite. Non-local models of thermal energy transport are becoming more popular for describing small-scale and/or high frequency thermodynamic processes and further testing of fractional models based on the fading memory concept is recommended. As discussed in section 2.1, this approach shares key features with the constitutive flux equation.

5.0 REFERENCES

1. S. Botelho-Andrade, E. Ahmed, and A. Wharmby, "Laser-tissue heating model modernization assessment, AFRL-RH-FS-TR-2023-0012," 711 HPW/RHDO, Tech. Rep., 2023 1, 22.

2. C. Cattaneo, "A form of heat-conduction equations which eliminates the paradox of instantaneous propagation," *Comptes Rendus*, vol. 247, p. 431, 1958 1, 4, 7, 8.

3. P. Vernotte, "Les paradoxes de la theorie continue de l'equation de la chaleur," *Comptes rendus*, vol. 246, p. 3154, 1958 1, 4, 7, 8.

4. K. Mitra, S. Kumar, A. Vedevarz, and M. Moallemi, "Experimental evidence of hyperbolic heat conduction in processed meat," *Journal of Heat Transfer*, vol. 117, no. 3, pp. 568–573, 1995 1, 4, 7, 9, 22.

5. A. Richardson, C. Imig, B. Feucht, and H. Hines, "The relationship between deep tissue temperature and blood flow during electromagnetic irradiation·," *Archives of Physical Medicine*, vol. 31, pp. 19–25, 1950 1.

6. R. Roemer, J. Oleson, and T. Cetas, "Oscillatory temperature response to constant power applied to canine muscle," *American Journal of Physiology-Regulatory, Integrative and Comparative Physiology*, vol. 249, no. 2, R153–R158, 1985 1.

7. B. Coleman, "Thermodynamics of materials with memory," *Arch. Rational Mech. Anal*, vol. 17, no. 1, pp. 1–46, 1964 2.

8. C.-C. Wang and R. Bowen, "On the thermodynamics of non-linear materials with quasi-elastic response," *Archive for Rational Mechanics and Analysis*, vol. 22, pp. 79–99, 1966 2.

9. M. Gurtin and A. Pipkin, "A general theory of heat conduction with finite wave speeds," *Archive for Rational Mechanics and Analysis*, vol. 31, pp. 113–126, 1968 2, 3, 28.

10. B. Coleman and W. Noll, "Foundations of linear viscoelasticity," *Reviews of modern physics*, vol. 33, no. 2, p. 239, 1961 2.

11. B. Coleman and M. Gurtin, "Equipresence and constitutive equations for rigid heat conductors," *Zeitschrift für angewandte Mathematik und Physik ZAMP*, vol. 18, no. 2, pp. 199–208, 1967 2.

12. J. Liu, "Preliminary survey on the mechanisms of the wave-like behaviors of heat transfer in living tissues," *Forschung im Ingenieurwesen*, vol. 66, no. 1, pp. 1–10, 2000 4, 9, 10.

13. Ş. Özen, S. Helhel, and O. Cerezci, "Heat analysis of biological tissue exposed to microwave by using thermal wave model of bio-heat transfer (twmbt)," *Burns*, vol. 34, no. 1, pp. 45–49, 2008 4.

14. L. Xu and J. Liu, "Discussion of non-equilibrium heat transfer in biological systems," in *ASME International Mechanical Engineering Congress and Exposition*, American Society of Mechanical Engineers, vol. 15984, 1998, pp. 13–17 4.

15. L. Boltzmann, "Zur theorie der elastischen nachwirkung," *Annalen der Physik*, vol. 241, no. 11, pp. 430–432, 1878 5.

16. L. Ferrás, N. Ford, M. Morgado, J. Nóbrega, and M. Rebelo, "Fractional pennes' bioheat equation: Theoretical and numerical studies," *Fractional Calculus and Applied Analysis*, vol. 18, pp. 1080–1106, 2015 5.

17. J. Hristov, "Bio-heat models revisited: Concepts, derivations, nondimensalization and fractionalization approaches," *Frontiers in Physics*, vol. 7, p. 189, 2019 5, 6.

18. D. Joseph and L. Preziosi, "Heat waves," *Reviews of Modern Physics*, vol. 61, no. 1, p. 41, 1989 6.

19. A. Araújo, J. Ferreira, and P. Oliveira, "The effect of memory terms in diffusion phenomena," *Journal of Computational Mathematics*, pp. 91–102, 2006 6.

20. K. Diethelm, *The analysis of fractional differential equations: an application-oriented exposition using differential operators of Caputo type*. Springer Berlin, 2010, vol. 2004 6.

21. C. Lane, H. Fairbank, and W. Fairbank, "Second sound in liquid helium ii," *Physical Review*, vol. 71, no. 9, p. 600, 1947 6.

22. M. Chester, "Second sound in solids," *Physical Review*, vol. 131, no. 5, p. 2013, 1963 6–8.

23. J. Ward and J. Wilks, "The velocity of second sound in liquid helium near the absolute zero," *The London, Edinburgh, and Dublin Philosophical Magazine and Journal of Science*, vol. 42, no. 326, pp. 314–316, 1951 6.

24. V. Peshkov, *Report on an international conference on fundamental particles and low temperature physics*, 1947 6.

25. J. Maxwell, "On the dynamical theory of gases," *Philosophical transactions of the Royal Society of London*, no. 157, pp. 49–88, 1867 7.

26. D. S. Chandrasekharaiah, "Hyperbolic thermoelasticity: A review of recent literature," *Applied Mechanics Reviews*, vol. 51, no. 12, pp. 705–729, 1998 7.

27. C. Christov, "On frame indifferent formulation of the maxwell–cattaneo model of finite-speed heat conduction," *Mechanics Research Communications*, vol. 36, no. 4, pp. 481–486, 2009 7.

28. D. Tzou, *Macro- To Micro-Scale Heat Transfer: The Lagging Behavior*. Taylor and Francis, New York, 1997 7, 9.

29. J. Liu, Z. Ren, and W. C., "Interpretation of living tissue's temperature oscillations by thermal wave theory," *Science Bulletin : English Version*, no. 17, pp. 1493–1495, 1995 7.

30. J. Ziman, *Electrons and phonons: the theory of transport phenomena in solids*. Oxford university press, 2001 8.

31. F. Seitz and D. Turnbull, *Solid state physics*. Academic Press, 1958 8.

32. L. Wang, X. Zhou, and X. Wei, *Heat conduction: mathematical models and analytical solutions*. Springer Science & Business Media, 2007 9.

33. W. Kaminski, "Hyperbolic heat conduction equation for materials with a nonhomogeneous inner structure," *J. Heat Transfer*, 1990 9.

34. W. Roetzel, N. Putra, and S. Das, "Experiment and analysis for non-fourier conduction in materials with non-homogeneous inner structure," *International Journal of Thermal Sciences*, vol. 42, no. 6, pp. 541–552, 2003 9.

35. H. Herwig and K. Beckert, "Experimental evidence about the controversy concerning fourier or non-fourier heat conduction in materials with a nonhomogeneous inner structure," *Heat and Mass Transfer*, vol. 36, no. 5, pp. 387–392, 2000 9.

36. A. Graßmann and F. Peters, "Experimental investigation of heat conduction in wet sand," *Heat and Mass Transfer*, vol. 35, no. 4, pp. 289–294, 1999 9.

37. D. Tzou, "Thermal shock phenomena under high rate response in solids," *Annual review of heat transfer*, vol. 4, 1992 9, 22.

38. M. Fabrizio and F. Franchi, "Delayed thermal models: Stability and thermodynamics," *Journal of Thermal Stresses*, vol. 37, no. 2, pp. 160–173, 2014 9.

39. M. Fabrizio and A. Morro, "Viscoelastic relaxation functions compatible with thermodynamics," *Journal of elasticity*, vol. 19, no. 1, pp. 63–75, 1988 9.

40. M. Fabrizio and A. Morro, "Dissipativity and irreversibility of electromagnetic systems," *Mathematical Models and Methods in Applied Sciences*, vol. 10, no. 02, pp. 217–246, 2000 9.

41. D. Tzou, "A unified field approach for heat conduction from macro-to micro-scales," *Journal of heat transfer*, 1995 10.

42. M. DeLisi, N. Gamez, C. Clark III, S. Kumru, B. Rockwell, and R. Thomas, "Computational modeling and damage threshold prediction of continuous-wave and multiple-pulse porcine skin laser exposures at 1070 nm," *Journal of Laser Applications*, vol. 33, no. 2, p. 022 023, 2021 10, 13, 16.

43. J. Lepock, H. Frey, and K. Ritchie, "Protein denaturation in intact hepatocytes and isolated cellular organelles during heat shock," *The Journal of cell biology*, vol. 122, no. 6, pp. 1267–1276, 1993 16, 22.

44. S. Prahl, "A monte carlo model of light propagation in tissue," in *Dosimetry of laser radiation in medicine and biology*, International Society for Optics and Photonics, vol. 10305, 1989, p. 1 030 509 20.

45. J. Hristov, “Transient heat diffusion with a non-singular fading memory: From the cattaneo constitutive equation with jeffrey’s kernel to the caputo-fabrizio time-fractional derivative,” *Thermal science*, vol. 20, no. 2, pp. 757–762, 2016 22.

46. J. Lepock, “Cellular effects of hyperthermia: Relevance to the minimum dose for thermal damage,” *International journal of hyperthermia*, vol. 19, no. 3, pp. 252–266, 2003 22.

APPENDIX A - BACKGROUND AND NOTATION FOR DERIVING CONSTITUTIVE FLUX EQUATION (3)

Let H (or $\mathbf{H}$) denote the set of all measurable real-valued (or vector-valued) functions f on $[0,\infty)$ with $\|f\| < \infty$ (as in equation (2)). Let H^+ denote the cone (in H) of essentially strictly positive functions and H^{++} denote the cone (in H^+) of essentially strictly monotone increasing functions.

The main result in [9] deals with constitutive equations of the following form

$$\psi(t) = \Psi(\theta, \overline{\theta}^t, \overline{\mathbf{g}}^t),$$

where Ψ is a smooth scalar-valued functional on $\mathbb{R}^+ \times H^{++} \times \mathbf{H}$. In the context of this report, $\theta = T$ and $\mathbf{g} = \nabla T$ and the history functions are defined in equation (1) of the main report.

Definition 1. *A pair $[\theta(\cdot), \mathbf{g}(\cdot)]$ of functions on $\mathbb{R}$ is called admissible if:*

i. $\theta(\cdot)$ *is continuous and piecewise smooth;*

ii. *is piecewise continuous;*

iii. $\theta^t \in H^+, \overline{\theta}^t \in H^{++}$ *and* $\mathbf{g}^t, \overline{\mathbf{g}}^t$ *for all* $t \in \mathbb{R}$.

In [9], a thermodynamic process is defined as an ordered array $[\theta(\cdot), \mathbf{g}(\cdot), \psi(\cdot), \eta(\cdot), \mathbf{q}(\cdot)]$ where $[\theta(\cdot), \mathbf{g}(\cdot)]$ is an admissible pair and $\psi(\cdot), \eta(\cdot)$, and $\mathbf{q}(\cdot)$ are defined by the functionals of the free energy, entropy, and heat flux discussed in Section 2.1.

Since Ψ is smooth, it has a partial derivative with respect to θ, $D_\theta \Psi(\theta, \overline{\theta}^t, \overline{\mathbf{g}}^t)$ (treating the other two terms as fixed), and has partial Fréchet derivatives:

$$\delta_1 \Psi(\theta, \overline{\theta}^t, \overline{\mathbf{g}}^t) : H \longrightarrow \mathbb{R}$$

with respect to $\overline{\theta}^t$ (treating θ and $\overline{\mathbf{g}}^t$ as fixed) and

$$\delta_2 \Psi(\theta, \overline{\theta}^t, \overline{\mathbf{g}}^t) : \mathbf{H} \longrightarrow \mathbb{R}$$

with respect to $\overline{\mathbf{g}}^t$ (treating θ and $\overline{\theta}^t$ as fixed). The formal definition of a Fréchet derivative is defined below.

Definition 2. *Let V and W be normed spaces with open subset $U \subseteq V$. A function $f : U \longrightarrow W$ is called Fréchet differentiable at $x \in U$ if there exists a bounded linear operator $A : V \longrightarrow W$ such that*

$$\lim_{\|h\| \to 0} \frac{\|f(x+h) - f(x) - Ah\|_W}{\|h\|_V} = 0. \tag{A-1}$$

Equation A-1. Fréchet Derivative

The operator A, if it exists, is the Fréchet derivative and is sometimes denoted as $f'(x)$.

It should be mentioned that equation (2) is the usual norm for the weighted L^p space $L^p_h(G)$ $(p=2)$ where h is sometimes considered to be a Beurling weight and G is a locally compact Abelian (or commutative) group. The term Beurling algebra is used for various algebras introduced by Arne Beurling (1949) that are closely related to the Wiener algebra. Typically it is an algebra consisting of periodic functions with Fourier series $f(x) = \sum a_n e^{inx}$. One commonly used type of Beurling weight satisfies the properties $h(s+t) \leq h(s)h(t)$ and $h(t) \geq 1$. It is relatively easy to show that a function that is monotonically decreasing and satisfies $h(x) \geq 1$ also satisfies $h(s+t) \leq h(s)h(t)$. However, the assumption that $h(t) \geq 1$ is incompatible with assuming $s^2 h(s)$ is integrable on $[0,\infty)$.

It should be mentioned that, while the norm in equation (2) looks like the weighted L^p norm, this is not the traditional weighted L^p space referenced in most literature. Recall that L^p represents a space of measurable functions for which the p-th power of the absolute value is Lebesgue integrable, or

$$\|f\|_p = \left(\int_0^\infty |f(s)|^p \, ds \right)^{1/p} < \infty, \tag{A-2}$$

Equation A-2. L^p **Norm**

where $1 \leq p < \infty$. Then the norm in equation (2) looks identical to the norm of the weighted L^2 space with weight $h(s)$, often denoted L^p_h, but in this case the weights being considered are different.

LIST OF SYMBOLS, ABBREVIATIONS, AND ACRONYMS

$\mathbf{q_{con}}$	The converted energy flux or the flux that is induced by the heat transport but does not appear in the form of heat.
κ	Thermal conductivity.
α	The order of a fractional derivative of fractional integral.
ρ	Density of the tissue.
$\alpha_{\mathbf{Epidermis}}(T)$	Optical absorption coefficient of the epidermis layer.
τ_T	The phase lag time for the temperature gradient.
ω_b	The blood perfusion rate coefficient.
$\|\|f\|\|$	Weighted L^p norm with Beurling weight h.
$C_{\mathbf{Epidermis}}(T)$	Specific heat of the epidermis layer.
$T(\vec{r},t)$	The temperature at position $\vec{r}$ and time t.
T_b	The temperature of the perfused blood.
c	The specific heat of the tissue.
c_b	The specific heat of the perfused blood.
$\mathbf{q}(\vec{r},t)$	The heat flux at position $\vec{r}$ and time t.
DPL	Dual Phase Lag
ED50	The laser injury threshold identified as the effective dose required for 50% probability of damage
MVL	Minimum Visible Lesion
SESE	Scalable Effects Simulation Environment
TWMBT	Thermal Wave Model for Bioheat Transfer